Mech. Sci., 17, 759–767, 2026
https://doi.org/10.5194/ms-17-759-2026

Mechanical Sciences
Open Access

Trajectory-tracking control of the UR10 manipulator based on radial basis function neural network and super-twisting sliding mode

Xiaole Ma, Chenghu Jing, Kun Zhang, Chen Chen, and Yanfeng Wang

School of Mechanical and Electrical Engineering, Henan University of Technology, Zhengzhou 450001, China

Correspondence: Chenghu Jing (chhjing@haut.edu.cn)

Received: 13 April 2026 – Revised: 5 June 2026 – Accepted: 6 July 2026 – Published: 27 July 2026

Abstract. This paper proposes a composite control strategy combining a radial basis function (RBF) neural network and super-twisting sliding-mode control for high-precision trajectory tracking of the UR10 manipulator under parameter variations, nonlinear friction, and external disturbances. An RBF network is employed to approximate the lumped unknown nonlinear dynamics online, thereby reducing the equivalent disturbance upper bounds. Simultaneously, a super-twisting robust control term is introduced to compensate for approximation residuals and remaining disturbances, which ensures system robustness while effectively suppressing conventional sliding-mode chattering. Furthermore, a projection-based adaptive law is designed to guarantee the strict boundedness of the network weights. Based on Lyapunov theory, the finite-time convergence of the sliding variable and tracking error is proven. Simulations on a 6-degree-of-freedom UR10 manipulator – incorporating mass/inertia perturbations and Coulomb-viscous friction – demonstrate that the proposed method achieves high-precision tracking with small steady-state errors and smooth, chattering-free control torques, verifying its effectiveness and engineering applicability.

1 Introduction

Robotic manipulators are strongly coupled, nonlinear systems widely applied in industrial manufacturing, medical assistance, and special operations (Liu et al., 2023). With the growing demand for human–robot collaboration, collaborative robots have become essential as they share workspaces with humans without physical separation (Matheson et al., 2019; Taesi et al., 2023). However, practical operations often suffer from parameter uncertainties, nonlinear friction, and external disturbances, which can degrade tracking accuracy and compromise system stability (Spong, 2022).

Sliding-mode control (SMC) is widely used due to its desirable robustness against matched disturbances (Hashimoto et al., 1987). Yet, the discontinuous switching in conventional SMC induces high-frequency chattering, exciting unmodeled dynamics and increasing actuator wear (Uyulan, 2022). Higher-order SMC, particularly the super-twisting algorithm, generates continuous control inputs to suppress chattering while achieving robust finite-time convergence (Al-Dujaili et al., 2020; Goel and Swarup, 2017; Zhai and Li, 2022; Sun et al., 2024). Nevertheless, under strong unknown nonlinearities, relying solely on super-twisting requires large control gains, increasing energy consumption and risking actuator torque saturation (Ai et al., 2026).

Neural-network approximation effectively compensates for unknown dynamics (Abdallah and Fareh, 2019). Radial basis function (RBF) networks are widely adopted due to their simple structure and linear parameterization (Moosavi et al., 2022; Dinh et al., 2008). Combining an RBF network with SMC forms a "feedforward approximation + robust compensation" framework: the network approximates dominant nonlinearities to reduce sliding-mode gains, while the SMC handles residual errors and disturbances (Zhao et al., 2025; Wai, 2003; Zhang and Qian, 2025; Lin et al., 2025). Furthermore, since conventional adaptive laws often overcomplicate Lyapunov derivations and easily cause weight drift (Ren et al., 2020), a hard projection operator is introduced to keep weight estimates bounded and improve numerical stability (Agarwal and Parthasarathy, 2016).

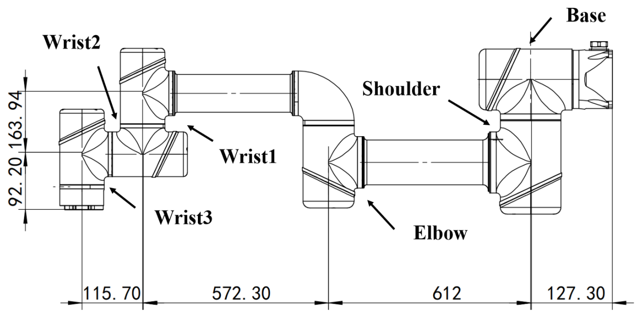

Figure 1. UR10 kinematic model.

Inspired by super-twisting strategies demonstrating superior anti-disturbance performance in specialized equipment (Liu et al., 2026; Mou and Wu, 2020; Ren et al., 2023; Chen et al., 2025; Dirara et al., 2025), this paper develops a composite control strategy for the UR10 manipulator. The main contributions are summarized as follows: (1) establishing a UR10 dynamics model considering nonlinear friction and parameter uncertainties; (2) proposing a composite RBF and super-twisting SMC law with a projection-based adaptive operator; (3) proving finite-time convergence of the sliding variable via Lyapunov analysis; and (4) demonstrating superiority over standalone RBF and SMC methods in tracking accuracy, chattering suppression, and robustness via simulations.

2 Dynamics model and problem formulation

The UR10 is a widely studied 6-degree-of-freedom collaborative robot (Fig. 1) (Petrone et al., 2025). Its dynamics can be expressed as follows:

$$\mathbf{M}(\boldsymbol{q})\ddot{\boldsymbol{q}} + \mathbf{C}(\boldsymbol{q},\dot{\boldsymbol{q}})\dot{\boldsymbol{q}} + \mathbf{G}(\boldsymbol{q}) + \boldsymbol{\tau}_{\mathrm{f}}(\dot{\boldsymbol{q}}) = \boldsymbol{\tau} + \boldsymbol{\tau}_{\mathrm{d}}, \tag{1}$$

where $\mathbf{M}(\boldsymbol{q}) \in \mathbb{R}^{n\times n}$, $\mathbf{C}(\boldsymbol{q},\dot{\boldsymbol{q}}) \in \mathbb{R}^{n\times n}$, and $\mathbf{G}(\boldsymbol{q}) \in \mathbb{R}^{n}$ are the inertia, Coriolis or centrifugal, and gravity matrices, respectively; $\boldsymbol{\tau}_{\mathrm{d}} \in \mathbb{R}^{n}$ is the external disturbance; $\boldsymbol{\tau}_{\mathrm{f}}(\dot{\boldsymbol{q}})$ is the nonlinear joint friction; $\boldsymbol{q} \in \mathbb{R}^{n}$ is the joint position; and $\boldsymbol{\tau} \in \mathbb{R}^{n}$ is the control input.

In practical applications, decomposing actual parameters into nominal values and uncertainties, Eq. (1) can be rewritten as follows:

$$\mathbf{M}_0(\boldsymbol{q})\ddot{\boldsymbol{q}} + \mathbf{C}_0(\boldsymbol{q},\dot{\boldsymbol{q}})\dot{\boldsymbol{q}} + \mathbf{G}_0(\boldsymbol{q}) = \boldsymbol{\tau} + \boldsymbol{f}(\boldsymbol{x}) + \boldsymbol{\tau}_{\mathrm{d}}, \tag{2}$$

where $\boldsymbol{x} = \left[\boldsymbol{q}^T, \dot{\boldsymbol{q}}^T\right]^T$ is the system state, and $\boldsymbol{f}(\boldsymbol{x}) = -\Delta\mathbf{M}(\boldsymbol{q})\ddot{\boldsymbol{q}} - \Delta\mathbf{C}(\boldsymbol{q},\dot{\boldsymbol{q}})\dot{\boldsymbol{q}} - \Delta\mathbf{G}(\boldsymbol{q}) + \boldsymbol{\tau}_{\mathrm{f}}(\dot{\boldsymbol{q}})$ represents the lumped unknown dynamics, including unmodeled friction and parameter uncertainties; quantities with the subscript "0" denote nominal values, and those with "Δ" represent parametric uncertainties.

Property 1. The inertia matrix $\mathbf{M}_0(\boldsymbol{q})$ is symmetric positive definite and satisfies $m_{\min} \le \|\mathbf{M}_0(\boldsymbol{q})\| \le m_{\max}$, $\forall \boldsymbol{q} \in \mathbb{R}^{n}$, where $m_{\min}$ and $m_{\max}$ are positive constants.

Assumption 1. The desired trajectory $\boldsymbol{q}_{\mathrm{d}}$ and its derivatives $\dot{\boldsymbol{q}}_{\mathrm{d}}$ and $\ddot{\boldsymbol{q}}_{\mathrm{d}}$ are continuous and uniformly bounded. Furthermore, the initial system state $\boldsymbol{x}(0) = \left[\boldsymbol{q}^T(0), \dot{\boldsymbol{q}}^T(0)\right]^T$ is assumed to belong to a known compact set Ω_x.

Remark 1. This assumption replaces the conventional "$\boldsymbol{q}, \dot{\boldsymbol{q}}$ are bounded" assumption, thereby avoiding the circular argument that presupposes boundedness before proving stability. Assuming the initial state lies in a compact set is a rigorous mathematical prerequisite for ensuring the universal approximation property of the subsequent radial basis function neural network within its effective domain.

To handle the unknown nonlinear function $\boldsymbol{f}(\boldsymbol{x})$, an RBF neural network is introduced for approximation. For any continuous function $\boldsymbol{f}(\boldsymbol{x})$, within a compact set, it can be modeled by an ideal neural network as follows:

$$\boldsymbol{f}(\boldsymbol{x}) = \mathbf{W}^{*T}\boldsymbol{\Phi}(\boldsymbol{x}) + \boldsymbol{\varepsilon}(\boldsymbol{x}), \tag{3}$$

where $\mathbf{W}^* \in \mathbb{R}^{N\times n}$ is the ideal weight matrix, $\boldsymbol{\Phi}(\boldsymbol{x}) \in \mathbb{R}^{N}$ is the Gaussian radial basis functions vector, N is the number of hidden-layer nodes, and $\boldsymbol{\varepsilon}(\boldsymbol{x}) \in \mathbb{R}^{n}$ is the network approximation error.

Assumption 2. The ideal weight matrix $\mathbf{W}^*$ and the approximation error $\boldsymbol{\varepsilon}(\boldsymbol{x})$ are bounded, i.e., $\|\mathbf{W}^*\|_{\mathrm{F}} \le W_M$ and $\|\boldsymbol{\varepsilon}(\boldsymbol{x})\| \le \varepsilon_M$. Moreover, the Gaussian basis functions themselves are bounded, satisfying $\|\boldsymbol{\Phi}(\boldsymbol{x})\| \le \sqrt{N}$. The external disturbance $\boldsymbol{\tau}_{\mathrm{d}}$ is also bounded.

Remark 2. In this paper, for a vector $\boldsymbol{s} = [s_1, s_2, \ldots, s_n]^T$, the symbol $|\boldsymbol{s}|^{1/2}\mathrm{sign}(\boldsymbol{s})$ denotes element-wise operation, i.e., $[|s_1|^{1/2}\mathrm{sign}(s_1), \ldots, |s_n|^{1/2}\mathrm{sign}(s_n)]^T$.

3 Adaptive super-twisting decoupled control design and stability analysis

3.1 Controller and adaptive law design

We define the trajectory-tracking error as $\boldsymbol{e} = \boldsymbol{q} - \boldsymbol{q}_{\mathrm{d}}$ and construct a linear sliding surface:

$$\boldsymbol{s} = \dot{\boldsymbol{e}} + \boldsymbol{\Lambda}\boldsymbol{e}, \tag{4}$$

where $\boldsymbol{\Lambda} = \mathrm{diag}\{\lambda_1, \ldots, \lambda_n\}$ is a positive definite diagonal matrix. Differentiating Eq. (4) and substituting into Eq. (2) yields the sliding-surface dynamics:

$$\begin{aligned}\mathbf{M}_0(\boldsymbol{q})\dot{\boldsymbol{s}} =& \mathbf{M}_0(\boldsymbol{q})(\ddot{\boldsymbol{q}} - \ddot{\boldsymbol{q}}_{\mathrm{d}} + \boldsymbol{\Lambda}\dot{\boldsymbol{e}}) \\ =& \boldsymbol{\tau} + \boldsymbol{f}(\boldsymbol{x}) + \boldsymbol{\tau}_{\mathrm{d}} - \mathbf{C}_0\dot{\boldsymbol{q}} - \mathbf{G}_0 \\ & - \mathbf{M}_0(\boldsymbol{q})(\ddot{\boldsymbol{q}}_{\mathrm{d}} - \boldsymbol{\Lambda}\dot{\boldsymbol{e}}).\end{aligned} \tag{5}$$

To achieve high-precision tracking and eliminate chattering, an RBF-based super-twisting sliding-mode control (RBF-STSMC) is designed:

$$\begin{aligned}\boldsymbol{\tau} =& \mathbf{M}_0(\boldsymbol{q})(\ddot{\boldsymbol{q}}_{\mathrm{d}} - \boldsymbol{\Lambda}\dot{\boldsymbol{e}}) + \mathbf{C}_0(\boldsymbol{q},\dot{\boldsymbol{q}})\dot{\boldsymbol{q}} + \mathbf{G}_0(\boldsymbol{q}) - \widehat{\mathbf{W}}^T\boldsymbol{\Phi}(\boldsymbol{x}) \\ & + \mathbf{M}_0(\boldsymbol{q})\boldsymbol{u}_{\mathrm{st}},\end{aligned} \tag{6}$$

where $\widehat{\mathbf{W}} \in \mathbb{R}^{N\times n}$ is the estimated weight matrix of the RBF neural network, used for feedforward compensation of system uncertainties, and $\boldsymbol{u}_{\mathrm{st}} \in \mathbb{R}^n$ is the super-twisting robust control term, designed to suppress residual errors and external disturbances. The design of $\boldsymbol{u}_{\mathrm{st}}$ is as follows:

$$\boldsymbol{u}_{\mathrm{st}} = -\boldsymbol{\alpha}|\boldsymbol{s}|^{1/2}\mathrm{sign}(\boldsymbol{s}) - \boldsymbol{\beta}\int \mathrm{sign}(\boldsymbol{s})\mathrm{d}t, \tag{7}$$

with $\boldsymbol{\alpha} = \mathrm{diag}\{\alpha_1,\ldots,\alpha_n\}$ and $\boldsymbol{\beta} = \mathrm{diag}\{\beta_1,\ldots,\beta_n\}$ being diagonal matrices of positive control gains.

To ensure boundedness of the neural network weights and to avoid a stringent cancellation design in the Lyapunov derivative, a hard projection operator is introduced for the weight adaptation law. Let the raw update direction matrix be $\mathbf{Y} = \boldsymbol{\Gamma}\boldsymbol{\Phi}(\boldsymbol{x})\boldsymbol{s}^T$. The adaptive law is as follows:

$$\begin{aligned}\dot{\widehat{\mathbf{W}}} &= \mathrm{Proj}(\widehat{\mathbf{W}},\mathbf{Y})\\ &= \begin{cases} \mathbf{Y}, & \|\widehat{\mathbf{W}}\|_{\mathrm{F}} < W_{\max} \text{ or} \\ & (\|\widehat{\mathbf{W}}\|_{\mathrm{F}} = W_{\max} \text{ and } \mathrm{tr}(\widehat{\mathbf{W}}^T\mathbf{Y}) \le 0) \\ \mathbf{Y} - \frac{\mathrm{tr}(\widehat{\mathbf{W}}^T\mathbf{Y})}{\|\widehat{\mathbf{W}}\|_{\mathrm{F}}^2}\widehat{\mathbf{W}}, & \|\widehat{\mathbf{W}}\|_{\mathrm{F}} = W_{\max} \text{ and } \mathrm{tr}(\widehat{\mathbf{W}}^T\mathbf{Y}) > 0 \end{cases},\end{aligned} \tag{8}$$

where $\boldsymbol{\Gamma}$ is a positive learning rate matrix, $\mathrm{tr}(\cdot)$ denotes the matrix trace, and $\|\cdot\|_{\mathrm{F}}$ is the Frobenius norm.

Remark 3. When the norm of the estimated weights $\|\widehat{\mathbf{W}}\|_{\mathrm{F}}$ reaches the preset safety boundary $W_{\max}$ and the update direction continues to point outward, the outward normal update component is forcibly removed, limiting the update direction to the tangent of the boundary. This mathematically guarantees globally and strictly that $\|\widehat{\mathbf{W}}\|_{\mathrm{F}} \le W_{\max}$ holds at all times.

To intuitively illustrate the overall architecture of the proposed RBF-STSMC, the complete system block diagram is depicted in Fig. 2. As shown in the figure, the composite control law is driven by the tracking error and the sliding variable. It consists of three primary modules: the nominal dynamic compensation based on prior knowledge, the RBF neural network feedforward term for online approximation of unknown dynamics, and the super-twisting robust term designed to suppress chattering and reject residual disturbances.

3.2 Closed-loop system restatement and disturbance boundedness analysis

Substituting the control law Eq. (6) into Eq. (5) yields the closed-loop sliding-surface dynamics:

$$\dot{\boldsymbol{s}} = -\widetilde{\mathbf{W}}^T\boldsymbol{\Phi}(\boldsymbol{x}) + \boldsymbol{\delta}(t) + \boldsymbol{u}_{\mathrm{st}}, \tag{9}$$

where $\widetilde{\mathbf{W}} = \widehat{\mathbf{W}} - \mathbf{W}^*$ is the weight estimation error, and $\boldsymbol{\delta}(t) = \mathbf{M}_0^{-1}(\boldsymbol{q})(\boldsymbol{\varepsilon}(\boldsymbol{x}) + \boldsymbol{\tau}_{\mathrm{d}})$ is a bounded composite term comprising the network approximation error and external disturbance.

We define the total lumped disturbance on the sliding surface as $\boldsymbol{\Delta}_{\mathrm{total}}(t) = -\widetilde{\mathbf{W}}^T\boldsymbol{\Phi}(\boldsymbol{x}) + \boldsymbol{\delta}(t)$. Given the projection operator ($\|\widehat{\mathbf{W}}\|_{\mathrm{F}} \le W_{\max}$) and assumption 2, the ith component of $\boldsymbol{\Delta}_{\mathrm{total}}(t)$ strictly satisfies

$$|\Delta_{\mathrm{total},i}(t)| \le L_i, \tag{10}$$

where $L_i > 0$ is an existing but unknown constant bound, providing a rigorous prerequisite for robust control.

3.3 Finite-time convergence proof of the super-twisting algorithm

Theorem 1. We consider system (2) to satisfy assumptions 1–2. Under the sliding surface (4), control law (6)–(7), and adaptive law (8), if the gains α_i and β_i satisfy certain conditions then the sliding variable $\boldsymbol{s}$ converges to the origin in finite time.

Proof. We write the i subsystem dynamics in the standard super-twisting form:

$$\begin{cases} \dot{s}_i = -\alpha_i|s_i|^{1/2}\mathrm{sign}(s_i) + v_i + \Delta_{\mathrm{total},i}(t) \\ \dot{v}_i = -\beta_i\,\mathrm{sign}(s_i) \end{cases}, \tag{11}$$

where v_i is the super-twisting integral state. From Eq. (10), the disturbance satisfies $|\Delta_{\mathrm{total},i}(t)| \le L_i$.

We construct the transformed state vector $\boldsymbol{\zeta}_i = [\zeta_{i1},\zeta_{i2}]^T = \left[|s_i|^{1/2}\mathrm{sign}(s_i), v_i\right]^T$. Differentiating and writing in a matrix form gives

$$\dot{\boldsymbol{\zeta}}_i = \frac{1}{2|\zeta_{i1}|}\left(\mathbf{A}_i\boldsymbol{\zeta}_i + \mathbf{B}\Delta_{\mathrm{total},i}(t)\right), \tag{12}$$

where

$$\mathbf{A}_i = \begin{bmatrix} -\alpha_i & 1 \\ -2\beta_i & 0 \end{bmatrix}, \quad \mathbf{B} = \begin{bmatrix} 1 \\ 0 \end{bmatrix}.$$

We consider the strongly robust Lyapunov function,

$$V_i(\boldsymbol{\zeta}_i) = \boldsymbol{\zeta}_i^T\mathbf{P}_i\boldsymbol{\zeta}_i, \tag{13}$$

with

$$\mathbf{P}_i = \frac{1}{2}\begin{bmatrix} 4\beta_i + \alpha_i^2 & -\alpha_i \\ -\alpha_i & 2 \end{bmatrix},$$

to be strictly symmetric positive definite. Differentiating V_i along the system trajectory yields the following:

$$\begin{aligned}\dot{V}_i =& \frac{1}{2|\zeta_{i1}|}\boldsymbol{\zeta}_i^T\left(\mathbf{A}_i^T\mathbf{P}_i + \mathbf{P}_i\mathbf{A}_i\right)\boldsymbol{\zeta}_i \\ &+ \frac{1}{|\zeta_{i1}|}\Delta_{\mathrm{total},i}(t)\mathbf{B}^T\mathbf{P}_i\boldsymbol{\zeta}_i.\end{aligned} \tag{14}$$

Since $|\Delta_{\mathrm{total},i}(t)| \le L_i$, algebraic bounding arguments show that if the control gains satisfy

$$\alpha_i > 1.5\sqrt{L_i}, \quad \beta_i > 1.1L_i \tag{15}$$

then there exists a positive definite matrix $\widetilde{\boldsymbol{Q}}_i > 0$ such that

$$\dot{V}_i \le -\frac{1}{2|\zeta_{i1}|}\boldsymbol{\zeta}_i^T\widetilde{\boldsymbol{Q}}_i\boldsymbol{\zeta}_i \le -\frac{\lambda_{\min}(\widetilde{\boldsymbol{Q}}_i)}{2|\zeta_{i1}|}\|\boldsymbol{\zeta}_i\|^2. \tag{16}$$

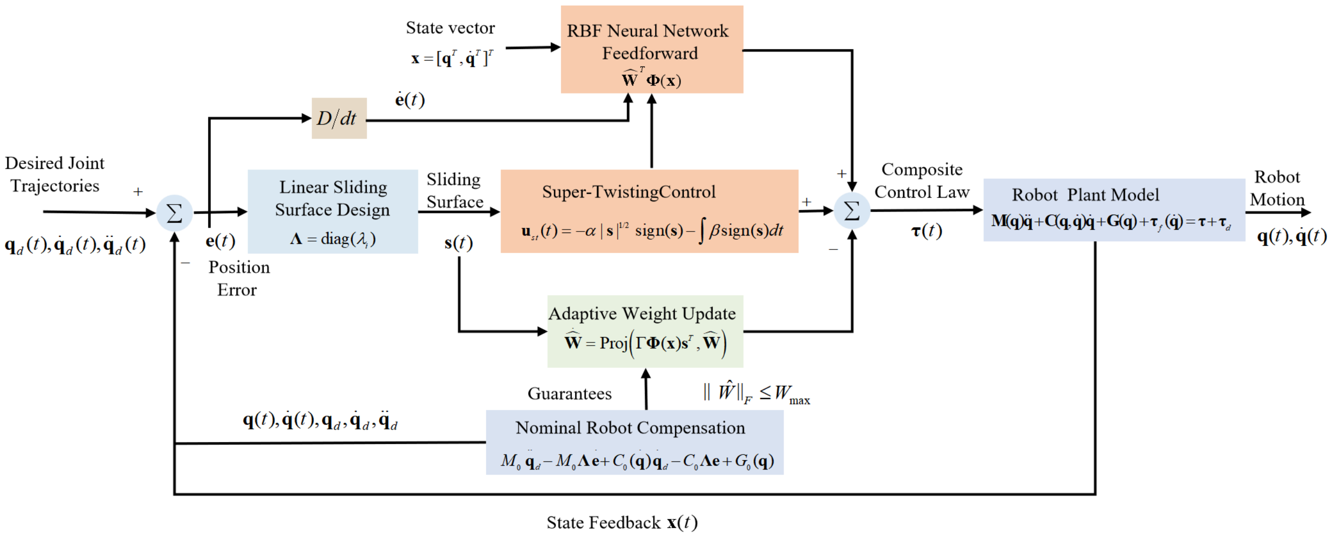

Figure 2. Block diagram of the proposed RBF-STSMC control system.

Using Rayleigh quotient inequalities $\lambda_{\min}(\mathbf{P}_i)\|\boldsymbol{\zeta}_i\|^2 \le V_i \le \lambda_{\max}(\mathbf{P}_i)\|\boldsymbol{\zeta}_i\|^2$ and the fact that $|\zeta_{i1}| \le \|\boldsymbol{\zeta}_i\| \le \sqrt{V_i/\lambda_{\min}(\mathbf{P}_i)}$, we obtain

$$\dot{V}_i \le -\gamma_i V_i^{1/2}, \tag{17}$$

where

$$\gamma_i = \frac{\lambda_{\min}(\widetilde{\boldsymbol{Q}}_i)}{\lambda_{\max^{1/2}}(\mathbf{P}_i)\sqrt{\lambda_{\max}(\mathbf{P}_i)}} > 0.$$

By the Lyapunov finite-time stability comparison lemma, Eq. (17) implies that V_i converges to zero in finite time $T_r \le \frac{2V_i^{1/2}(0)}{\gamma_i}$. Consequently, the transformed state $\boldsymbol{\zeta}_i$ (i.e., s_i and v_i) converges to the origin in finite time. Then, from the linear sliding surface of Eq. (4), the tracking error $\boldsymbol{e}$ converges asymptotically to zero.

Remark 4. Conventional adaptive SMC often uses the adaptive law to exactly cancel uncertainty terms, easily leading to gain drift. In contrast, the decoupled proof framework adopted here utilizes the RBF network to physically reduce the total disturbance bound $\boldsymbol{L}$. Consequently, the required super-twisting gains ($\boldsymbol{\alpha}$, $\boldsymbol{\beta}$) can be substantially relaxed, effectively reducing energy consumption and chattering while maintaining finite-time stability guarantees.

4 Simulation verification

4.1 Simulation object and parameter settings

The UR10 6-degree-of-freedom manipulator is taken as the simulation object, and the nominal dynamic parameters are adopted from the experimental identification results reported in Petrone et al. (2025). To simulate parameter uncertainties, the actual model introduces perturbations on the basis of the nominal one: the masses of joints 2 and 3 are increased by 20 %, the centers of mass are shifted, and the inertia is increased by 5 %, while joint 6 remains at its nominal value to reflect asymmetric uncertainty. To accurately capture the nonlinear friction characteristics (e.g., Coulomb and viscous friction) while avoiding the numerical chattering and algebraic loops caused by discontinuous signum functions in simulations, a smooth sigmoidal friction model is introduced. The friction torque $\tau_{\mathrm{f,i}}(\dot{\boldsymbol{q}}_i)$ for the ith joint is formulated as $\tau_{\mathrm{f,i}}(\dot{\boldsymbol{q}}_i) = c_{i,1} + c_{i,1}\dot{\boldsymbol{q}}_i + \frac{c_{i,3}}{1+e^{-c_{i,4}(\dot{\boldsymbol{q}}_i + c_{i,5})}}$, where $\dot{\boldsymbol{q}}_i$ is the joint velocity, and $c_{i,1}$ to $c_{i,5}$ are the identified friction coefficients for each joint. Based on experimental data, the coefficient vectors $\boldsymbol{c}_i = [c_{i,1}, c_{i,2}, c_{i,3}, c_{i,4}, c_{i,5}]$ for joints 1 to 6 are set as follows: joint 1 – [1.064, −1.006, 2.050, 7.946, −0.018]; joint 2 – [0.994, 0.956, −2.401, −59.953, −0.001]; joint 3 – [0.679, −0.812, 1.647, 19.825, −0.005]; joint 4 – [0.315, −0.176, 0.468, 134.898, −0.018]; joint 5 – [0.224, −0.192, 0.476, 331.442, −0.011]; and joint 6 – [0.235, −0.245, 0.598, 459.193, −0.013].

The external disturbance is defined as $\boldsymbol{\tau}_{\mathrm{d}} = 0.5\sin(2\pi t)\cdot \boldsymbol{I}_6$ N m. The disturbance amplitude of 0.5 N m is selected to represent typical unmodeled torques and load fluctuations. As shown in Fig. 3, a fixed-gain study with disturbance amplitudes of 0.1, 0.5, and 2.0 N m reveals that the method maintains reliable tracking (RMSE < 0.005 rad) for disturbances up to at least 2.0 N m. For larger disturbances, the gains can be adjusted using Eq. (15) based on the estimated upper bound of the total disturbance L_i.

The desired trajectory starts from the initial pose $\boldsymbol{q}_0 = [0, -\pi/2, 0, -\pi/2, 0, 0]^T$ rad and moves to the target pose $\boldsymbol{q}_{\mathrm{f}} = [0.316, 0.672, 0.506, 0.672, 0, 1.255]^T$ rad. A fifth-order polynomial trajectory is adopted, with a motion duration of $T = 10$ s and a control period of $\mathrm{d}t = 0.001$ s. To prevent numerical overflow of the in-

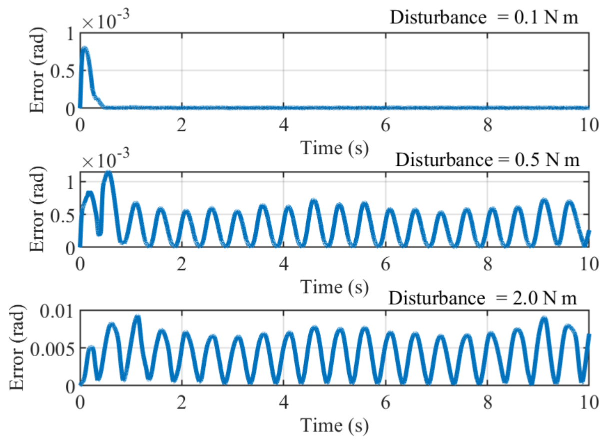

Figure 3. Effect of disturbance amplitude on tracking error.

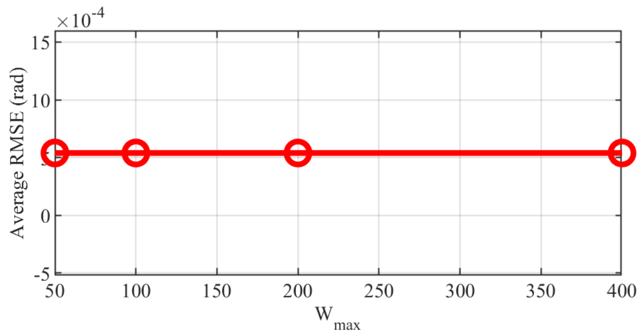

Figure 4. Sensitivity of tracking error to $W_{\max}$.

tegral term in the super-twisting control (Eq. 7), saturation limits of $\pm 100\,\mathrm{N\,m}$ are applied to the integral state during the discrete-time simulation using Euler integration with step size $\mathrm{d}t = 0.001\,\mathrm{s}$. The controller parameters are as follows: $\boldsymbol{\Lambda} = \mathrm{diag}(30, 30, 30, 25, 25, 40)$; super-twisting gains $\boldsymbol{\alpha} = \mathrm{diag}(10, 10, 10, 25, 25, 80)$, $\boldsymbol{\beta} = \mathrm{diag}(20, 20, 20, 50, 50, 150)$; RBF network hidden layer nodes $N = 120$; centers are obtained by K-means clustering from trajectory data; widths are set to the average distance between all centers; learning rate $\boldsymbol{\Gamma} = 0.5\boldsymbol{I}$; and weight upper bound $W_{\max} = 200$. The weight upper bound $W_{\max} = 200$ is empirically chosen based on the estimated Frobenius norm of the ideal weight matrix. As shown in Fig. 4, a sensitivity analysis with $W_{\max} = 50$, 100, 200, and 400 shows that the average tracking RMSE remains 0.00054 rad, indicating that the control performance is largely insensitive to $W_{\max}$ as long as it is set sufficiently large.

4.2 Simulation Results and Analysis

Figure 5 shows the time evolution of position tracking errors for each joint under three control schemes: pure RBF, SMC, and the proposed composite RBF-STSMC strategy. Under pure RBF control, the lack of a sliding-mode robust term leads to significant deterioration in tracking accuracy when facing parameter perturbations and external disturbances. As shown in Fig. 5a, the steady-state errors of joints 4, 5, and 6 are as high as 0.7108, 0.8159, and 0.4795 rad, respectively, while their maximum tracking errors reach 1.2001, 0.8865, and 1.0151 rad. This indicates that an RBF neural network alone lacks effective disturbance rejection capability without sliding-mode compensation. The SMC strategy achieves significantly better tracking accuracy due to the robust action of its fixed-gain switching term; as shown in Fig. 5b, the steady-state errors of joints 4 and 5 drop to 0.0011 and 0.0077 rad, respectively. In contrast, the proposed RBF-STSMC composite strategy exhibits superior tracking accuracy on all joints. As shown in Fig. 5c, the steady-state errors of joints 4 and 5 are further reduced to 0.0005 and 0.0017 rad, representing improvements of over 50 % and 78 % compared to pure SMC, respectively. Except for joint 5, all other joints achieve steady-state errors better than 1×10^{-3} rad, strongly verifying the fast convergence and robust disturbance attenuation capability of the proposed method.

Figure 6 shows the time histories of the sliding variables s_i for each joint under the SMC and RBF-STSMC strategies. Both methods guarantee boundedness of the sliding variables. For the proposed RBF-STSMC composite strategy, the maximum absolute values $|s_i|$ of the sliding variables for joints 4, 5, and 6 are 0.1483, 0.1152, and 0.0592, respectively, whereas corresponding values for pure SMC are 0.2703, 0.9733, and 0.0639. Moreover, the composite method reduces the peak sliding variable of joint 5 by 88 %. The composite controller exhibits excellent transient response performance, with sliding-surface values being quickly constrained within a narrow boundary layer. This advantage stems from the finite-time convergence of the super-twisting control law and the RBF network's fast compensation for unknown nonlinearities. In contrast, although the pure SMC strategy eventually converges, its fixed-gain structure struggles to adapt to time-varying uncertainties, leading to larger transient deviations in the sliding surface.

As shown in Fig. 7, the maximum torque among the three methods occurs at joint 2, with values of 63.13 N m (RBF), 62.13 N m (SMC), and 62.24 N m (RBF-STSMC). All peak torques are well below the preset actuator saturation limits. However, the qualitative characteristics of the torque signals differ fundamentally. The proposed RBF-STSMC outputs a continuous and smooth control torque, free of the high-frequency chattering commonly observed in traditional SMC. It achieves significantly better tracking accuracy alongside smooth control signals, indicating strong engineering feasibility.

Figure 8 compares the evolution of the Frobenius norm of the RBF weight matrix under pure RBF and the proposed RBF-STSMC composite control configurations. Under pure RBF control, the weight norm exhibits a significant growth trend, reaching a final value of 5.72. This reflects the network's attempt to independently learn all unknown system

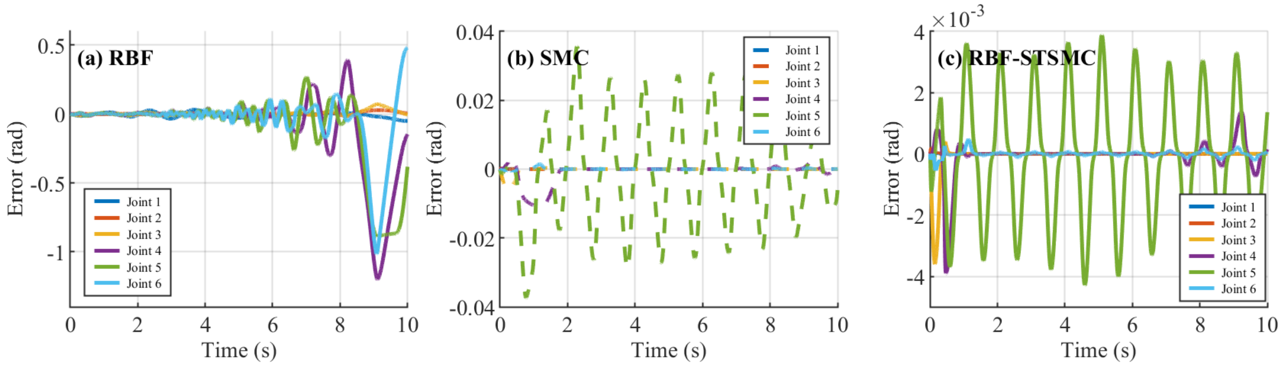

Figure 5. Joint position tracking error analysis.

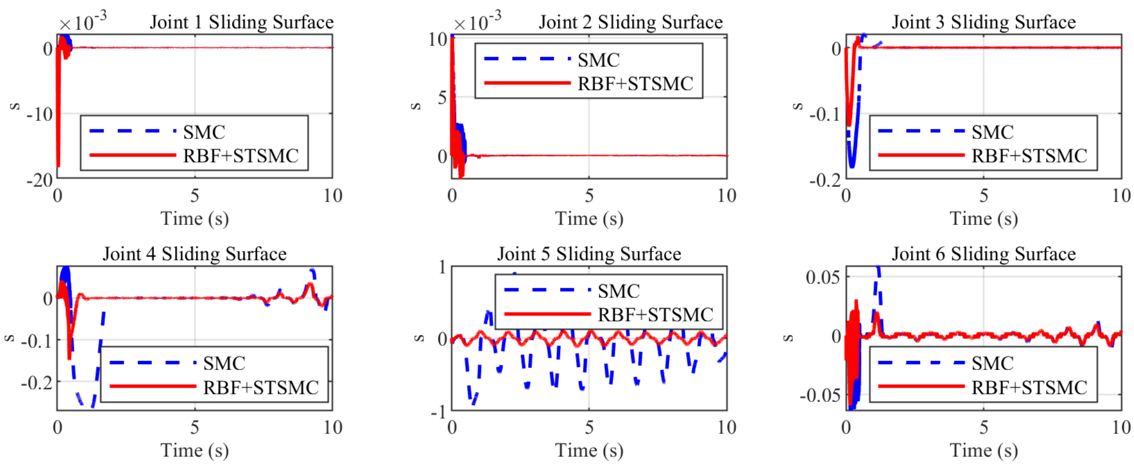

Figure 6. Analysis of sliding-mode surface convergence process.

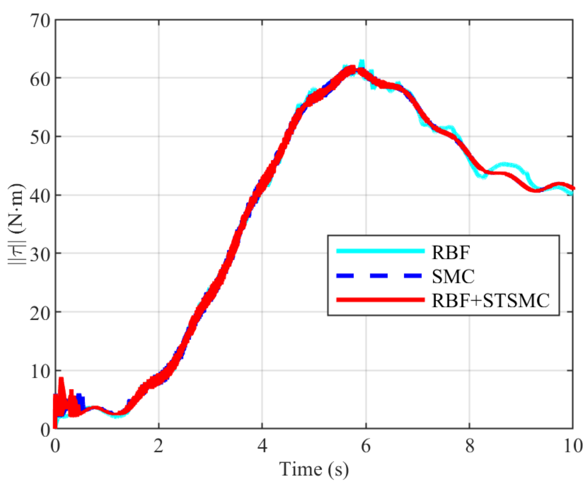

Figure 7. Analysis of control torque curve.

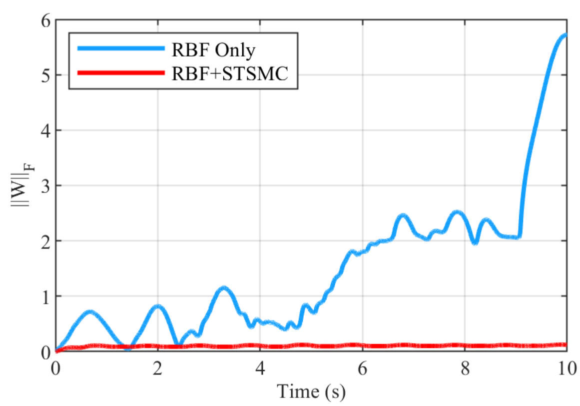

Figure 8. Evolution of neural network weight norm.

dynamics and disturbance characteristics without the aid of a robust control term. Under the proposed RBF-STSMC strategy, the weight norm stabilizes at 0.12 after an initial 3.7 s transient growth. This low norm value is attributed to effective synergy: the super-twisting sliding-mode term undertakes the main disturbance rejection task, thereby limiting the neural network's role to fine compensation of unmodeled dynamics.

Figure 9 shows the three-dimensional Cartesian space trajectory of the end effector. This simulation is a point-to-point

Table 1. ITAE values for each joint under different controllers.

Controller	J1 ITAE	J2 ITAE	J3 ITAE	J4 ITAE	J5 ITAE	J6 ITAE	Sum
RBF-STSMC	0.0	0.0	0.2	7.5	82.6	2.6	93.0
SMC	0.0	0.0	0.9	25.8	639.9	3.5	670.1
RBF	757.4	425.4	790.2	11997.7	12055.3	7491.1	33517.1

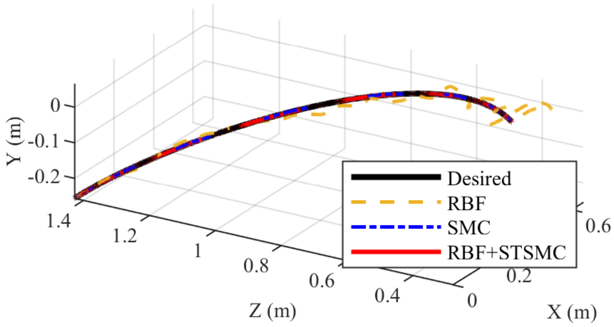

Figure 9. End effector trajectory.

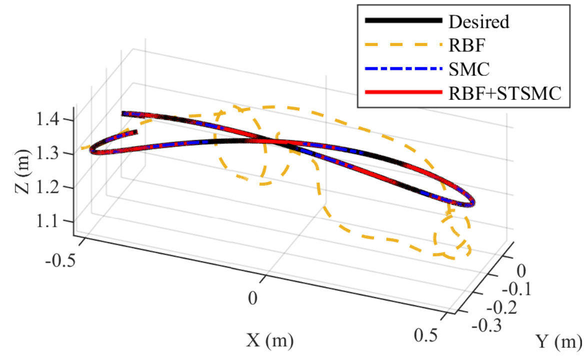

Figure 10. Tracking errors under continuous sinusoidal trajectory.

joint-space motion, with start and end points marked by a green circle and red triangle. The pure RBF controller yields an unacceptable steady-state Cartesian error of 0.1031 m, with a maximum deviation of 0.1444 m. The pure SMC method reduces the steady-state error to 0.0007 m, while the proposed RBF-STSMC composite method further improves it to 0.0002 m. These results fully confirm that the composite controller's joint-space error attenuation effectively transfers to the operational space, ensuring that the end effector tracks the prescribed path without noticeable overshoot or residual oscillation, ultimately achieving precise control.

To further quantify control performance, the integral of time-weighted absolute error (ITAE) is adopted as a comprehensive metric, defined as $\mathrm{ITAE} = \int_0^T t|e(t)|\mathrm{d}t$. A smaller ITAE value indicates better combined performance in terms of dynamic response speed and steady-state accuracy. The ITAE values for each joint are listed in Table 1.

Compared with pure SMC, the total ITAE of the RBF-STSMC controller is reduced by 86.1 %. In particular, the reductions for joints 5 and 4 reach 87.1 % and 70.9 %, respectively, indicating that the introduction of the RBF neural network effectively reduces the burden on the super-twisting gains and improves steady-state accuracy. Compared with pure RBF control, the total ITAE is reduced by as much as 99.7 %, fully demonstrating the necessity of the sliding-mode robust term in suppressing parameter perturbations and external disturbances. These results verify the superior performance of the proposed composite control strategy in terms of tracking speed and steady-state convergence accuracy.

To further demonstrate the generality of the proposed method beyond point-to-point motions, its tracking performance was also evaluated under a continuous sinusoidal trajectory. Each joint tracks an independent sinusoidal trajectory with different frequencies and amplitudes to simulate industrial continuous operation conditions.

Table 2. RMSE (rad) per joint under sinusoidal trajectory.

Method	J1	J2	J3	J4	J5	J6
RBF	0.169	0.191	0.515	9.592	2.454	12.989
SMC	0.000	0.000	0.000	0.004	0.016	0.001
RBF-STSMC	0.000	0.000	0.000	0.000	0.003	0.000

As shown in Fig. 10 and Table 2, the proposed RBF-STSMC controller maintains ultra-high tracking accuracy under periodic trajectories, with all joint RMSE values being less than 0.003 rad. Compared with SMC and pure RBF neural network control, the proposed method achieves significant improvements in tracking precision under continuous industrial motions. These results further verify the superior performance, generality, and robustness of the proposed composite control strategy.

5 Conclusion

This paper proposes a composite control strategy integrating an RBF neural network and super-twisting sliding-mode control for the high-precision trajectory tracking of the UR10 manipulator under parameter perturbations, nonlinear friction, and external disturbances. The RBF network online approximates unknown dynamics to reduce residual disturbance bounds, while the super-twisting term suppresses chattering and guarantees finite-time convergence, as rigorously proven via Lyapunov analysis. Additionally, a projection-based adaptive law strictly ensures weight boundedness. Simulations using realistic UR10 parameters demonstrate that this method significantly outperforms standalone SMC and RBF control regarding steady-state accuracy, convergence speed, and chattering suppression. Future work will focus on experimental validation on a physical UR10 platform, adaptive network structure optimization, and the integration of iterative learning with neural sliding-mode control.

Code and data availability. The code and data of this paper are available on request. Please contact the corresponding author.

Author contributions. Chenghu Jing: conceptualization and funding. Xiaole Ma: theoretical analysis and control design. Kun Zhang: simulations and writing of draft. Chen Chen: algorithm and data processing. Yanfeng Wang: conclusion and project coordination. All of the authors reviewed and approved the paper.

Competing interests. The contact author has declared that none of the authors has any competing interests.

Disclaimer. Publisher's note: Copernicus Publications remains neutral with regard to jurisdictional claims made in the text, published maps, institutional affiliations, or any other geographical representation in this paper. The authors bear the ultimate responsibility for providing appropriate place names. Views expressed in the text are those of the authors and do not necessarily reflect the views of the publisher.

Acknowledgements. We appreciate the editor Dario Richiedei and the reviewers for their valuable suggestions.

Financial support. This work was supported in part by the Natural Science Foundation of Henan Province, China (grant no. 262300421328).

Review statement. This paper was edited by Dario Richiedei and reviewed by two anonymous referees.

References

Abdallah, M. A. Y. and Fareh, R.: Tracking control of serial robot manipulator using active disturbance rejection control, 2019 Advances in Science and Engineering Technology International Conferences (ASET), 1–5, https://doi.org/10.1109/icaset.2019.8714470, 2019.

Agarwal, V. and Parthasarathy, H.: Disturbance estimator as a state observer with extended Kalman filter for robotic manipulator, Nonlinear Dynam., 85, 2809–2825, https://doi.org/10.1007/s11071-016-2864-4, 2016.

Ai, H.-B., He, X.-R., and Yin, C.-W.: Predefined-time super-twisting sliding mode control for construction robot with arbitrary initial values, Sensors, 26, 1654, https://doi.org/10.3390/s26051654, 2026.

Al-Dujaili, A. Q., Falah, A., Humaidi, A. J., Pereira, D. A., and Ibraheem, I. K.: Optimal super-twisting sliding mode control design of robot manipulator: Design and comparison study, Int. J. Adv. Robot. Syst., 17, 1729881420981524, https://doi.org/10.1177/1729881420981524, 2020.

Chen, J. Q., Zhang, H. Y., Pan, S. T., Zhu, T. T., and Lin, Y. Z.: A time-varying second-order sliding mode control of super-twisting based on radial basis function neural networks, J. Braz. Soc. Mech. Sci., 47, 6, https://doi.org/10.1007/s40430-025-05577-y, 2025.

Dinh, B. H., Dunnigan, M. W., and Reay, D. S.: A practical approach for position control of a robotic manipulator using a radial basis function network and a simple vision system, WSEAS Transactions on Systems and Control, 3, 289–298, 2008.

Dirara, H. G., Yareshe, F. T., and Abdissa, C. M.: Design and analysis of adaptive fuzzy super-twisting sliding mode controller for uncertain 2-DOF robotic manipulator, IEEE Access, 13, 110241–110254, https://doi.org/10.1109/ACCESS.2025.3581449, 2025.

Goel, A. and Swarup, A.: MIMO uncertain nonlinear system control via adaptive high-order super twisting sliding mode and its application to robotic manipulator, Journal of Control, Automation and Electrical Systems, 28, 36–49, https://doi.org/10.1007/s40313-016-0286-7, 2017.

Hashimoto, H., Maruyama, K., and Harashima, F.: A microprocessor-based robot manipulator control with sliding mode, IEEE T. Ind. Electron., IE-34, 11–18, https://doi.org/10.1109/TIE.1987.350917, 1987.

Lin, X., Li, J. Y., Song, Y. K., Liu, C. G., and Yang, T. Y.: Improved fast non-singular adaptive super-twisting sliding mode control based on radial basis function neural network approximation for robot joint module, ISA T., 167, 746–760, https://doi.org/10.1016/j.isatra.2025.08.037, 2025.

Liu, Y. L., Li, Y. M., Shi, S. Y., Li, C., and Yun, J. T.: Active disturbance rejection control for ladle masonry robotic arm based on fixed-time observer, Concurr. Comp.-Pract. E., 38, e70497, https://doi.org/10.1002/cpe.70497, 2026.

Liu, Z. B., Peng, K. R., Han, L. P., and Guan, S. C.: Modeling and control of robotic manipulators based on artificial neural networks: A review, IJST-T. Mech. Eng., 47, 1307–1347, https://doi.org/10.1007/s40997-023-00596-3, 2023.

Matheson, E., Minto, R., Zampieri, E. G. G., Faccio, M., and Rosati, G.: Human-robot collaboration in manufacturing applications: A review, Robotics, 8, 100, https://doi.org/10.3390/robotics8040100, 2019.

Moosavi, S. K. R., Zafar, M. H., and Sanfilippo, F.: Forward kinematic modelling with radial basis function neural network tuned with a novel meta-heuristic algorithm for robotic manipulators, Robotics, 11, 43, https://doi.org/10.3390/robotics11020043, 2022.

Mou, F. L. and Wu, D.: Active disturbance rejection sliding mode control for robot manipulation, Journal of Intelligent Manufacturing and Special Equipment, 1, 67–85, https://doi.org/10.1108/JIMSE-06-2020-0004, 2020.

Petrone, V., Ferrentino, E., and Chiacchio, P.: The dynamic model of the UR10 robot and its ROS2 integration, IEEE T. Ind. Inform., https://doi.org/10.1109/tii.2025.3534415, 2025.

Ren, B., Wang, Y., and Chen, J. Y.: Trajectory-tracking-based adaptive neural network sliding mode controller for robot manipulators, J. Comput. Inf. Sci. Eng., 20, 031009, https://doi.org/10.1115/1.4047073, 2020.

Ren, Z. X., Liu, X. X., and Peng, S. R.: Neural network based active disturbance rejection control for multi-joint robotic arm, 2023 CAA Symposium on Fault Detection, Supervision and Safety for Technical Processes (SAFEPROCESS), https://doi.org/10.1109/safeprocess58597.2023.10295853, 2023.

Spong, M. W.: An historical perspective on the control of robotic manipulators, Annual Review of Control, Robotics, and Autonomous Systems, 5, 1–31, https://doi.org/10.1146/annurev-control-042920-094829, 2022.

Sun, C. C., Huang, Z. M., and Wu, H. T.: Adaptive super-twisting global nonsingular terminal sliding mode control for robotic manipulators, Nonlinear Dynam., 112, 5379–5389, https://doi.org/10.1007/s11071-024-09305-4, 2024.

Taesi, C., Aggogeri, F., and Pellegrini, N.: COBOT applications: recent advances and challenges, Robotics, 12, 79, https://doi.org/10.3390/robotics12030079, 2023.

Uyulan, C.: Design and stability analysis of a robust-adaptive sliding mode control applied on a robot arm with flexible links, Vibration, 5, 1, https://doi.org/10.3390/vibration5010001, 2022.

Wai, R. J.: Tracking control based on neural network strategy for robot manipulator, Neurocomputing, 51, 425–445, https://doi.org/10.1016/S0925-2312(02)00626-4, 2003.

Zhai, J. Y. and Li, Z. Y.: Fast-exponential sliding mode control of robotic manipulator with super-twisting method, IEEE T. Circuits-II, 69, 489–493, https://doi.org/10.1109/tcsii.2021.3081147, 2022.

Zhang, Y. B. and Qian, C.: Super-twisting algorithm sliding mode control of flexible manipulators considering uncertainty, Appl. Sci., 16, 387, https://doi.org/10.3390/app16010387, 2025.

Zhao, J., Li, Y., Li, Y., Pei, B., Yu, Z., and Dong, Z.: A predefined-time radial basis function (RBF) neural network tracking control method considering actuator faults for a new type of spraying robot, Mech. Sci., 16, 51–60, https://doi.org/10.5194/ms-16-51-2025, 2025.